RSC Advances

PAPER

View Article Online
View Journal | View Issue

Cite this: *RSC Adv.*, 2023, **13**, 31704

Robust, self-adhesive and anti-bacterial silk-based LIG electrodes for electrophysiological monitoring†

Mohamed K. M. Abd-Elbaki,[a] Tamer Mosaad Ragab,[d] Naglaa E. R. Ismael*[a] and Ahmed S. G. Khalil *[bc]

Flexible wearable electrodes have been extensively used for obtaining electrophysiological signals towards smart health monitoring and disease diagnosis. Here, low-cost, and non-conductive silk fabric (SF) have been processed into highly conductive laser induced graphene (LIG) electrodes while maintaining the original structure of SF. A CO_2-pulsed laser was utilized to produce LIG-SF with controlled sheet resistance and mechanical properties. Laser processing of SFs under optimized conditions yielded LIG-SF electrodes with a high degree of homogeneity on both, top and bottom layers. Silk fibroin/Ca^{2+} adhesive layers effectively promoted the adhesive, anti-bacterial properties and provided a conformal contact of LIG-SF electrodes with human skin. Compared with conventional Ag/AgCl electrodes, LIG-SF electrodes possesses a much lower contact impedance in contact with human skin enabling highly stable electrophysiological signals recording. The applicability of adhesive LIG-SF electrodes to acquire electrocardiogram (ECG) signals was investigated. ECG signals recordings of adhesive LIG-SF electrodes showed excellent performance compared to conventional Ag/AgCl electrodes at intense body movements while running at different speeds for up to 9 km over a duration of 24 h. Therefore, our proposed adhesive LIG-SF electrodes can be applied for long-term personalized healthcare monitoring and sports management applications.

Received 22nd August 2023
Accepted 23rd October 2023

DOI: 10.1039/d3ra05730e

rsc.li/rsc-advances

1. Introduction

Electrophysiological signals are low-level electrical biopotentials that control the activity of most human body movements.[1] Electrophysiological signals can be produced from different body organs and tissues, for instance, electroencephalograms (EEG) produced from the brain,[2] electrocardiograms (ECG) produced from the heart,[3,4] and electromyograms (EMG) produced from muscle tissues.[5] The physiological status of these body organs and tissues can be reflected by the electrophysiological signals,[6,7] therefore, human biopotentials play a vital role in pathological disease diagnosis and human health monitoring.[8] Among them, ambulatory ECG directly controls myocardial conduction of the heart, consequently it can diagnose abnormal heart rhythms[9] and several cardiovascular diseases (CVDs) such as coronary artery disease (CAD),[10] which is the leading cause of human death around the world according to world health organization (WHO).[11]

The transduction of electrophysiological signals can be achieved by electrical interfacing with human skin *via* epidermal electrodes. Conventionally, commercial Ag/AgCl electrodes are frequently-used in biopotential recordings to attain electrophysiological signals. However, these Ag/AgCl electrodes suffer from plenty of limitations. For instance, they are wet electrodes that require a conductive gel to reduce the contact impedance and motion artifacts. However, the conductive gel suffers from dehydration over time resulting in increased contact impedance and reducing the quality of electrophysiological signals produced.[12] Additionally, under sweaty conditions, conductive gels can be swallowed while sweating and can cause severe skin irritation with prolonged use.[13] Moreover, Ag/AgCl electrodes are rigid in nature leading to instable contact with human skin during motion.[14] Although Ag/AgCl electrodes have high performance in recording biopotentials instantly at a resting state, the forementioned limitations hinder their long-term performance and limits their application in sports management.[15] Hence, there is an emerging need for developing skin-conformable dry electrodes for human biopotential recordings.

[a]*Zoology Department, Faculty of Science, Fayoum University, 63514 Fayoum, Egypt*
[b]*Physics Department, Environmental and Smart Technology Group, Faculty of Science, Fayoum University, 63514 Fayoum, Egypt. E-mail: asg05@fayoum.edu.eg*
[c]*Institute of Basic and Applied Sciences, Faculty of Engineering, Egypt-Japan University of Science and Technology (E-JUST), 179 New Borg El-Arab City, Egypt*
[d]*Department of Cardiology, Faculty of Medicine, Fayoum University, 63514 Fayoum, Egypt*

† Electronic supplementary information (ESI) available. See DOI: https://doi.org/10.1039/d3ra05730e

Over the past few years, flexible wearable epidermal electrodes resemble the new generation of wearable sensing platforms for personalized healthcare applications.[16,17] Extensive research efforts have been devoted to developing on-skin flexible wearable electrodes as they offer potential advantages over conventional rigid electrodes such as Ag/AgCl electrodes and stainless-steel electrodes. Flexible wearable epidermal electrodes offer a compliant and conformable interface with human skin providing a stable contact during motion artifacts, therefore, they became promising candidates for conformal, long-term, and real-time electrophysiological signals monitoring applications.[18–20] To constantly attain high-quality electrophysiological signals, ideal epidermal electrode properties such as superior conductivity/very low sheet resistance, low electrode-skin contact impedance, stretchability, mechanical softness, biocompatibility, high adhesion, and breathability are preferred.[21] Recently, several approaches have been introduced for the development of high-performance wearable epidermal electrodes such as metal thin film electrodes,[22,23] carbon material electrodes,[24–26] conductive elastomeric filaments (CEFs) electrodes,[27] metallic nanomaterials-based electrodes,[28,29] conductive polymers-based electrodes,[30,31] and hydrogel-based electrodes.[32,33] Zhao *et al.* introduced an ultra-conformal skin electrodes based on graphene and PEDOT:PSS for long-term electrophysiological monitoring.[34] Yoon *et al.* developed a multifunctional hybrid skin patch for ECG, sweat, glucose and PH monitoring.[35] Moreover, soft bioelectronic stickers had been developed by Lopes *et al.* with as an alternative for long-term biopotential recordings. The bioelectronic stickers were made of conductive composites that includes polydimethylsiloxane (PDMS) as a substrate incorporated with silver, carbon, and silver-coated nickel particles as conductive particles.[36] In addition, Tabasum *et al.* developed wearable microfluidic-based e-skin for *in situ* sweat measurements with real-time feedback.[37] Although current epidermal dry electrodes have super conductive and skin-compliant properties, they still have some drawbacks. Being based on artificial polymer substrates and filling materials, biocompatibility and air/water permeability issues may trigger inflammatory responses.[38–40] Therefore, alternatives with high biocompatibility and antibacterial properties are still needed.

Silk fibroin, a natural protein-based polymer produced by *B. mori* silkworms, has been extensively used in various biomedical applications. Biocompatible and biodegradable nature in addition to antibacterial properties of silk fibroin opens the opportunity for their candidacy in wearable epidermal electrode applications.[41–43] For instance, Yang *et al.* developed a biocompatible on-skin conformal and adhesive polymer electrodes (CAPE) that depend on silk/polypyrrole films through interfacial polymerization for long-term continuous electrophysiological monitoring.[44] Moreover, Meng *et al.* developed self-adhesive, biodegradable silk-based dry electrodes that consist of polypyrrole as a conductive layer combined with acid-modified silk/cellulose nanocrystal (CNC) films and an adhesive layer of Ca-modified silk fibroin for continuous epidermal electrophysiological monitoring.[45]

Silk fibroin fabrics have been used in textile industry for many years due to their high mechanical properties, softness, and high skin affinity.[46] SFs are composed of multilayer woven interconnected fiber network of high flexibility and many 3D micropores making SFs potential candidates for highly-sensitive and excellent air permeable epidermal electrodes.[47,48] Superior conductivity/low sheet resistance play a key role in the sensitivity of epidermal electrodes and provide a lower skin-electrode contact impedance.[21] Raw SFs are non-conductive in nature therefore, several approaches have been introduced to address this issue either *via* conductive coatings of SF by multiwalled carbon nanotubes (MWCNTs) as conductive fillers to produce conductive MWCNTs@silk fabric (CSF), molybdenum disulfide (MoS_2) and reduced graphene oxide (rGO) or *via* carbonization.[47,49–51] Laser irradiation is a simple, cost-effective and low-consumption method of carbonization in which a CO_2-pulsed laser is applied onto synthetic organic polymers to induce a photothermal conversion into LIG.[52] Over the past few years, LIG has been utilized in wearable bioelectronic applications that require high flexibility and versatility. Li *et al.* prepared a LIG on SFs for flexible strain sensor applications. SFs were treated by CO_2-pulsed laser with different optimization parameters and reached a minimum sheet resistance of 40 $\Omega\ sq^{-1}$.[53] In addition, flexible and robust dry electrodes have been prepared by Zahed *et al.* for long-term biopotential recording. LIG was prepare on polyimide (PI) sheet followed by spray coating *via* an electrically conductive polymer (PEDOT:PSS) to enhance the electrical conductivity of the produced LIG sheets.[54] LIG prepared in both cases has a relatively high sheet resistance/low conductivity, therefore, direct preparation of LIG with high conductivity/very low sheet resistance remains a challenge.

In this work, robust, self-adhesive and anti-bacterial silk-based LIG electrodes were developed for electrophysiological signals monitoring through a facile and cost-effective approach. LIG was prepared on SFs by a two-step carbonization approach. Natural SFs were pre-carbonized at 350 °C and then irritated with a CO_2-pulsed laser with optimized parameters that yielded a minimum sheet resistance and maintained the mechanical properties of SFs. The as-fabricated silk-based LIG electrodes showed a high performance for electrophysiological signals monitoring by attaining high quality ECG signals of a volunteer. The long-term performance of silk-based LIG electrodes were studied by continually recording ECG signals of a volunteer for 24 h as well as at different running speeds, hence, silk-based LIG electrodes shows a high potential for sports management applications.

2. Experimental section

2.1. Materials

Raw SFs with a thickness of 130 μm were purchased from local manufacturer. Cocoons of *B. mori* silkworm were obtained from a local supplier. Sodium carbonate anhydrous and calcium chloride ($CaCl_2$) were purchased from Loba chemie. Formic acid (99–100%) was purchased from Chem-Lab. Commercial Ag/AgCl electrodes (Fig. S1†) were obtained from BSS Medical Supply CO., China.

2.2. Carbonization of SFs

2.2.1. Carbonization *via* muffle furnace. Pristine SFs (P-SF) were cut into 10 cm^2 pieces and washed with DI water and ethanol, respectively. In a muffle furnace under air atmosphere, SFs were thermally treated at 150 °C for 1 h and then were heated to reach 350 °C and kept for 3 h at 350 °C. After that, the fabrics were cooled naturally to room temperature in order to obtain carbonized SF (C-SF).

2.2.2. Carbonization *via* chemical vapor deposition (CVD). In addition to carbonization by muffle furnace, SFs were also carbonized by a chemical vapor deposition (CVD) technique to be compared with muffle carbonized SFs.[55] Raw SFs were cut and washed by the same way as muffle furnace carbonization. Under argon (Ar) gas atmosphere, SFs were thermally treated from 25 °C to 350 °C with a temperature increase rate of 5 °C min^{-1}, and then kept at 350 °C for 1 h. After that, SFs were heated from 350 °C to 900 °C with a temperature increase rate of 5 °C min^{-1}, and then kept at 900 °C for 3 h. At the end, the fabrics were naturally cooled to room temperature.

2.2.3. Weight loss (%) calculation. Weight loss (%) of carbonized SFs prepared by both methods was evaluated using the following equation:

$$\text{Wight loss } (\%) = (W1 - W2)/W1 \times 100 \quad (1)$$

where $W1$ is the weight of the SFs before carbonization and $W2$ is the final weight of SFs after carbonization.

2.3. Fabrication of LIG on SFs

For the fabrication of a large-area LIG on SFs (LIG-SF), rectangular-shaped electrodes were designed *via* RDworks software with dimensions of 35 mm in length and 20 mm in width. Carbonized SFs were cut, mounted onto a glass substrate and fixed with an adhesive tape. CO_2-pulsed laser cutter machine (CX-6090) with a wavelength of 10.6 μm and a spot size of 200 μm was utilized to convert the non-conductive SFs into conductive LIG-SFs. Optimization of LIG-SF was achieved by controlling the laser parameters such as laser treatment power (W), focus distance (mm), scanning speed (mm s^{-1}) and laser path spacing (mm). All samples were treated at a scanning speed of 30 mm s^{-1}, a laser path spacing of 0.2 mm, a focus distance of 10 mm, and while varying the laser treatment power from 1 to 2.5 watt.

2.4. Fabrication of adhesive silk-based LIG electrodes

To achieve a highly-adhesive property of LIG-SF electrodes, adhesive silk solutions were prepared as follows. Silk cocoons were degummed (removal of sericin) following our recently published article.[56] Degummed silk fibers (0.6 g) and $CaCl_2$ (0.71 g) were dissolved in 10 ml of formic acid solution to yield a percentage ratio of 70 : 30 of silk : calcium ions (Ca^{2+}). Adhesive silk solutions were cast onto LIG-SFs and dried overnight to finally obtain highly-adhesive silk-based LIG electrodes.

Fig. 1 illustrates the whole fabrication process of adhesive LIG-SF electrodes. In summary, P-SF are washed and then carbonized in a conventional muffle furnace at 350 °C for 3 h. The non-conductive C-SF was treated by a CO_2-pulsed laser to form a conductive LIG-SF electrodes. Finally, adhesive LIG-SF electrodes were prepared by casting of silk/Ca^{2+}/F.A solution onto LIG-SF electrodes.

2.5. Electrical characterization of silk-based LIG electrodes

Contact impedance of adhesive LIG-SF electrodes was evaluated during contact on human skin as electrode-skin contact impedance. An electrochemical workstation (CHI660E, CHI Instruments) was utilized to measure the contact impedance in the frequency range from 1–1000 Hz with 100 mV potential amplitude. In both cases, two adhesive LIG-SF electrodes or commercial Ag/AgCl electrodes were placed onto forearm with a separating center to center distance of 8 cm.

2.6. Electrophysiological signals recording

Ambulatory ECG signals were recorded using a three-electrode system. Two adhesive LIG-SF electrodes were used as working electrodes, and one commercial Ag/AgCl electrode was used as a reference electrode. To acquire high quality ECG signals, electrodes were placed on the chest of a healthy volunteer (Male, 25 years old) and connected to an open-source monitoring system (AD8232 ECG sensor kit with an Arduino UNO R3 development board) by lead wires to successfully amplify and collect ECG signals.

2.7. Anti-bacterial activity measurements

Anti-bacterial properties of commercial Ag/AgCl, LIG-SF and adhesive LIG-SF electrodes were investigated *via* Kirby–Bauer test against Gram-positive *S. aureus*[57]. Recently cultured *S. aureus* in a nutrient broth solution was spread on top of sterilized agar plates with a medical swap. Three different bacterial-cultured agar plates were utilized for measuring the anti-bacterial activity of commercial Ag/AgCl, LIG-SF and adhesive LIG-SF electrodes, respectively. Another bacterial-cultured agar plate was utilized as a control plate. Then, all plates were incubated at 37 °C for 24 h to enhance the bacterial growth of *S. aureus.* After incubation, the diameter of inhibition zone was evaluated in order to investigate the antibacterial activity of commercial Ag/AgCl, LIG-SF and adhesive LIG-SF electrodes.

2.8. Characterization of P-SF, C-SF and LIG-SF

Structural characterization and morphology of P-SF, C-SF and LIG-SF were studied by a high-resolution SEM (ZEISS Sigma 500 VP) coupled with EDX detector for elemental mapping. Electrode-skin contact impedance was investigated *via* electrochemical workstation (CHI660E, CHI Instruments) at a frequency range from 1–1000 Hz with 100 mV potential amplitude. Sheet resistance of LIG-SF electrodes was measured by a parameter analyzer (Keithley 4200-SCS) *via* a four-probe method. Mechanical properties of LIG-SF electrodes were investigated by a mechanical tester (ZwickRoell Z010, Germany) with a 10 kN load cell. Large-area LIG-SF electrodes (35 mm in length and 20 mm in

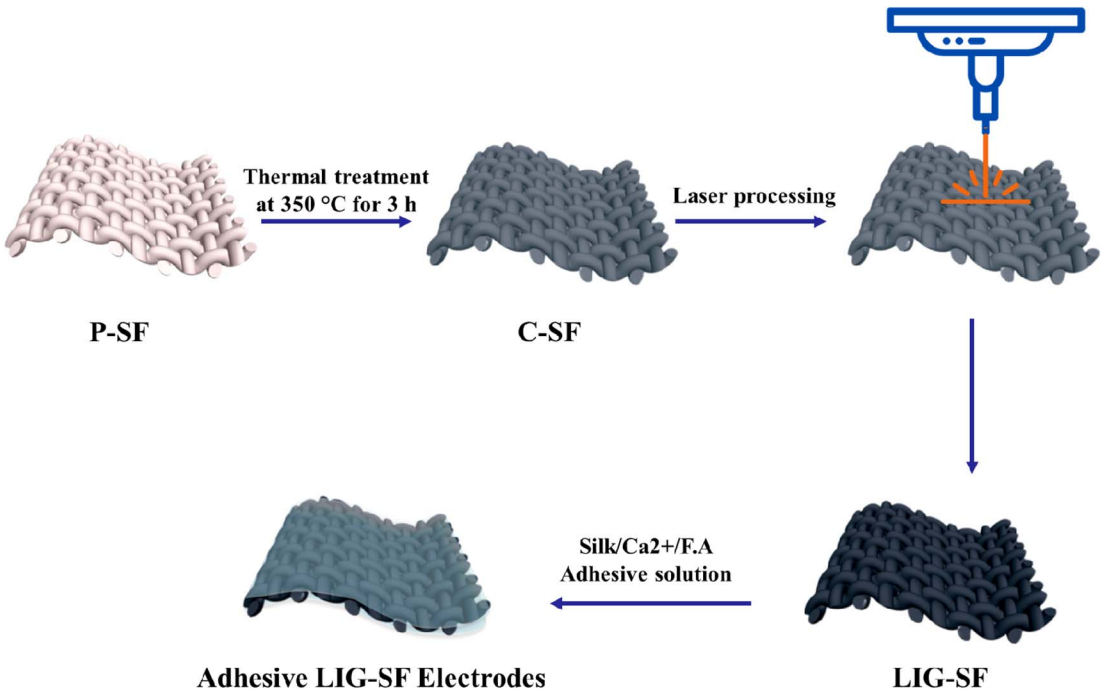

Fig. 1 Schematic illustration of the fabrication process of adhesive LIG-SF electrodes.

width) were placed between the grips with a grip-to-grip separation of 20 mm and measured with a speed rate of 40 mm min^{-1}. Adhesion force measurements were investigated *via* a standard 90°-peel test method. Adhesive LIG-SF electrodes with the same dimensions were mounted onto a glass or plastic substrate, connected at 90° with the mechanical grip and measured with a speed rate of 40 mm min^{-1}.

2.9. Ethical statement

All experiments were performed in accordance with the Guidelines of "Supreme Committee for Scientific Research Ethics (Code Number: EC 2211)", and approved by the ethics committee at Fayoum University, Egypt. Study participants were fully informed regarding the purposes of the study and consent was obtained.

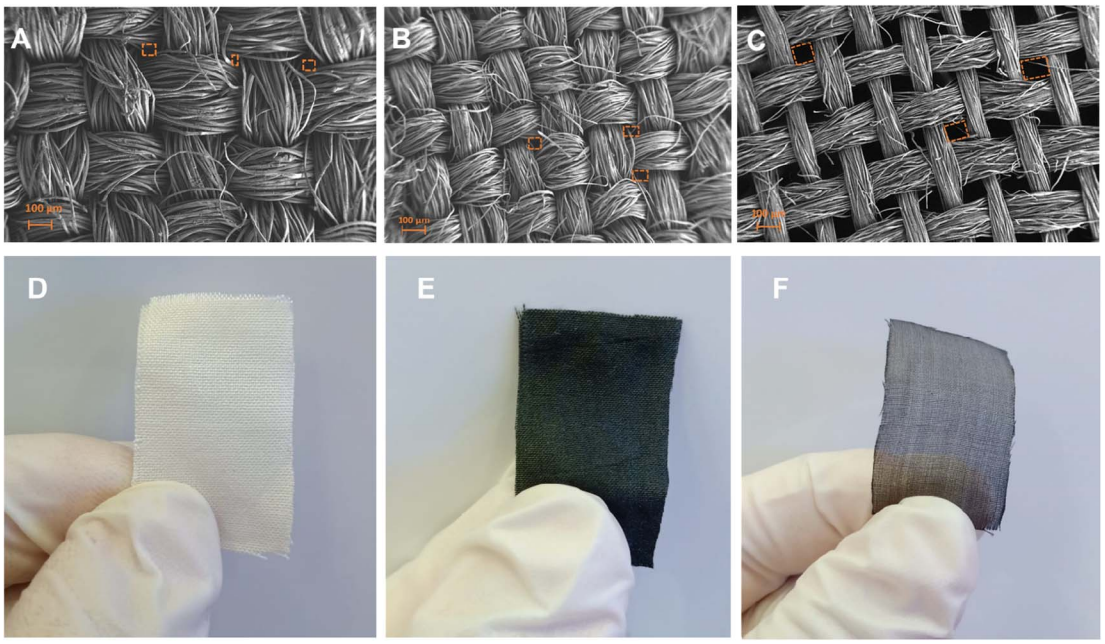

Fig. 2 (A–C) HR-SEM images and (D–F) digital photographs of P-SF, C-SF and LIG-SF, respectively.

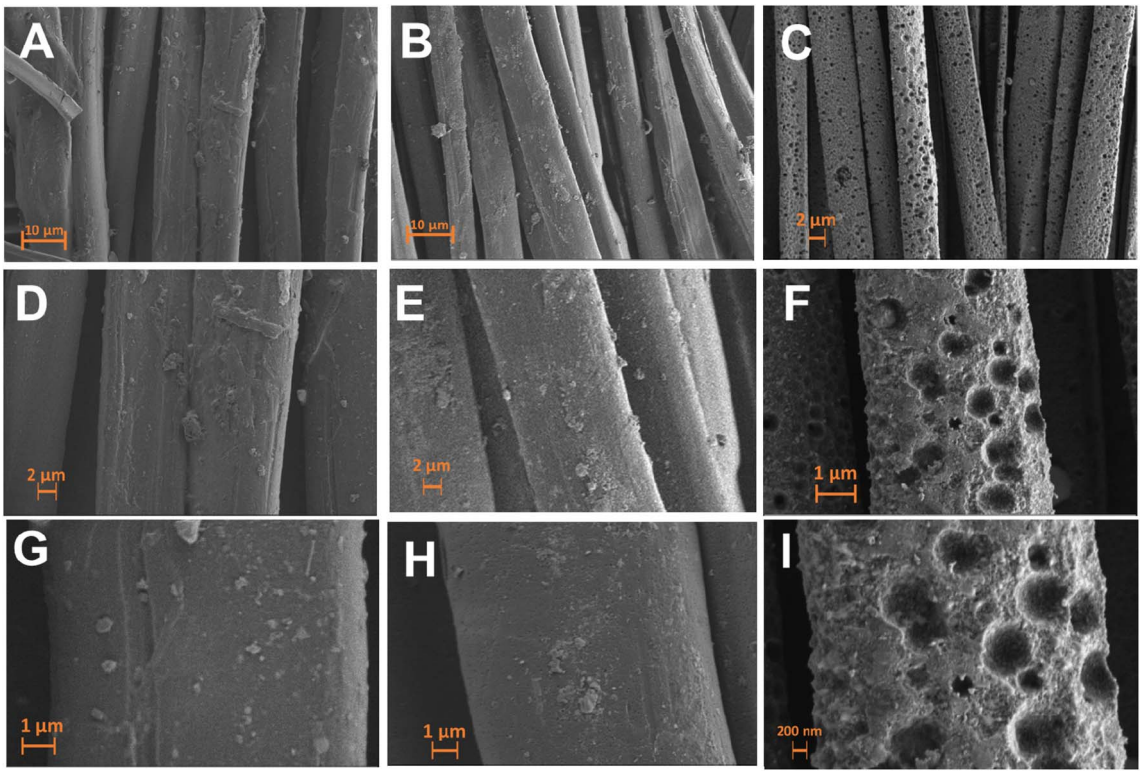

Fig. 3 HR-SEM images (A–C) bundle, (D–F) low magnification single fiber and (G–I) high magnification single fiber structures of P-SF, C-SF, and LIG-SF, respectively.

3. Result and discussion

3.1. Morphology and structural characterization of P-SF, C-SF, and LIG-SF

The surface morphology of pristine, carbonized and LIG-based SFs were studied *via* high resolution scanning electron microscopy (HR-SEM) as shown in Fig. 2. SEM images of pristine SFs (Fig. 2A) indicated a woven parallel interconnected fiber network gapped with numerous 3D micro-pores (highlighted in orange color). After carbonization at 350 °C for 3 h, C-SF reserved the same interconnected woven structure of P-SF, however, the diameter of silk fiber bundles was decreased (Fig. 2B). This may be attributed to the weight loss resulted by the carbonization process.[55] Laser treatment of C-SF lead to the formation of conductive LIG on SFs. Fig. 2C shows that LIG-SF still maintain the original interconnected woven structure of P-SF and C-SF. However, the diameter of silk fiber bundles was intensely decreased due to the high temperature induced by CO_2-pulsed laser treatment. As a result, the 3D micro-porous structure of LIG-SF strongly increased in diameter (Fig. 2C). Digital photographs of P-SF, C-SF and LIG-SF were used to observe color changes in each case. P-SF showed an original off-white color (Fig. 2D), however, after thermal treatment at 350 °C, a black-colored C-SF were obtained (Fig. 2E). This black color is mainly due to the sp^2-hybridized carbon structures induced by the carbonization process.[58] Digital photograph of LIG-SF showed a faint, black-colored fabrics with low transparency (Fig. 2F) which was mainly induced by the decrease in silk fiber bundles and the increase in pore size of the 3D micro-porous structure confirmed by HR-SEM images (Fig. 2C).

The microstructure of pristine, carbonized and LIG-based SFs were studied *via* HR-SEM images shown in Fig. 3. The bundle and single-fiber structure morphology of P-SF reveals a smooth surface of aligned silk fibers (Fig. 3A, D and G). The same was observed in C-SF with slight decrease in fiber diameter (Fig. 3B, E and H). On the other hand, the bundle and single-fiber structure morphology LIG-SF reveals that silk fibers were intensely decreased in diameter. In addition, LIG-SF showed a rough surface with the appearance of numerous micro-holes (Fig. 3C, F and I).

In addition, SEM images of fabric structures (Fig. 2 A–C) and bundle structures (Fig. 3 A–C) showed that P-SF, and C-SF are composed of interconnected fiber networks with little structural defects in single fibers that may be resulted during the fabric weaving process. Similarly, after laser processing, the same observation was shown in LIG-SF samples that showed nearly the same single fiber defects while maintaining the interconnected fiber network of fiber bundles, indicating that laser processing has no damaging effect on the optimized LIG-SF electrodes.

EDX elemental mapping of the pristine (Fig. 4 A–C), carbonized (Fig. 4 D–F), and LIG-based SFs (Fig. 4 G–I) indicated that all forms of SFs are mainly composed of carbon, oxygen and nitrogen with a uniform distribution. However, the atomic percentage for each element calculated by EDX were different (Table 1). The atomic percentage ratio of P-SF was noticed to be 51.14%, 27.1% and

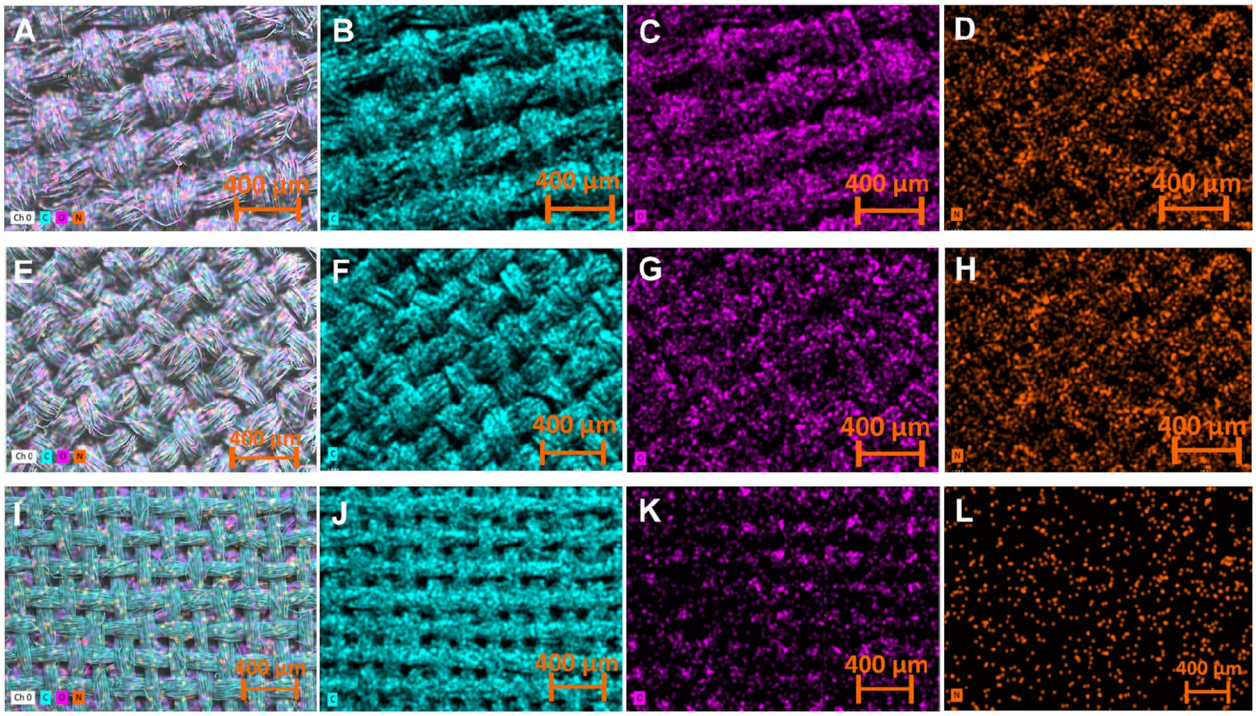

Fig. 4 EDX elemental mapping of P-SF (A–D), C-SF (E–H) and LIG-SF (I–L).

21.85% for carbon, oxygen and nitrogen, respectively. However, after carbonization at 350 °C for 3 h, the atomic percentage ratio of carbon in C-SF slightly increased to be 57.15%. In case of LIG-SF, the atomic percentage ratio of carbon intensely increased to be 88.43% and the atomic percentage ratio of oxygen and nitrogen were decreased to be 6.66% and 4.91%, respectively. This high atomic percentage ratio of carbon in LIG-SF confirms the successful transformation of non-conductive C-SF into conductive carbon-rich LIG on SFs.

Moreover, Raman spectroscopy was performed for P-SF, C-SF, and LIG-SF samples to confirm the structural changes resulted by both the carbonization and the laser treatment processes (Fig. 5). Raman spectrum of SF displayed peaks at 1083 cm^{-1}, 1227 cm^{-1} and 1663 cm^{-1} which are characteristic for β-sheet secondary structures, as well as the characteristic adsorption peak at 2933 cm^{-1} that represents CH stretching of silk proteins.[59,60] In case of C-SF, adsorption D, and G peaks appeared at 1351 cm^{-1} and 1551 cm^{-1} due to the carbonization process of silk fabrics. While in case of LIG-SF, both top and bottom sides of laser-treated fabrics showed the D, and G bands in addition to a characteristic broad 2D band at 2880 cm^{-1} which is attributed to second-order zone-boundary phonons of LIG-SF.[61,62]

Table 1 EDX atomic percentage ratio of P-SF, C-SF and LIG-SF

Elements	PSF	CSF	LIG-SF (top-side)	LIG-SF (back-side)
Carbon (C)	51.14	57.15	88.43	87.61
Oxygen (O_2)	27.01	13.37	6.66	6.62
Nitrogen (N_2)	21.85	29.48	4.91	5.76
Sum	100%			

3.2. Carbonization of SFs

Carbonization is a process by which natural organic polymers can be transformed into highly-rich carbon polymers *via* heat treatment at up to 800–3000 °C through removal of non-carbon polymeric elements in the form of volatile gases.[63] In this work, carbonization of SFs was achieved by two different approaches. First, SFs were thermally treated in a CVD at 350 °C for 1 h, followed by thermal treatment at 900 °C under argon

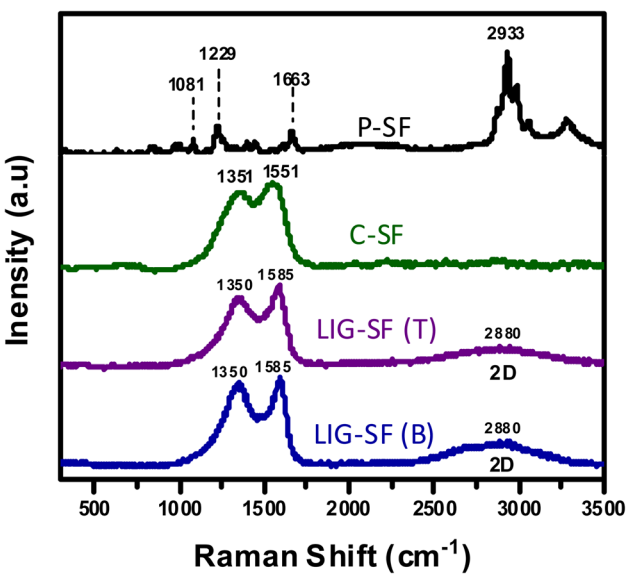

Fig. 5 Raman spectra of P-SF, C-SF, top layer of laser-treated fabrics (LIG-SF (T)), and bottom layer of laser-treated fabrics (LIG-SF (B)).

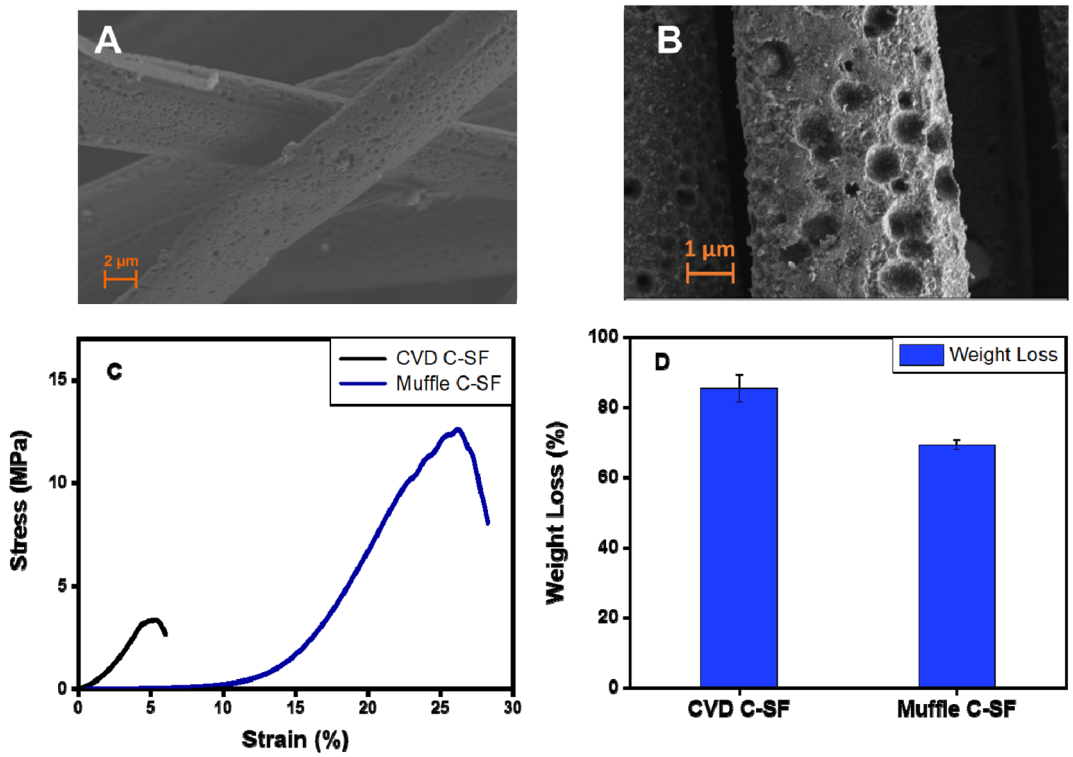

Fig. 6 (A and B) SEM image of CVD-carbonized and muffle-carbonized SFs, respectively. (C and D) Mechanical properties and weight loss % of CVD-carbonized and muffle-carbonized SFs, respectively.

atmosphere as a one-step carbonization approach. In the second approach, an ordinary muffle furnace was used for thermal treatment of SFs at 350 °C for 1 h, followed by laser treatment of C-SF to produce LIG-SF as a two-step carbonization approach. HR-SEM images of LIG-SF showed a rough surface with the presence of numerous micro-holes (Fig. 6B), similar

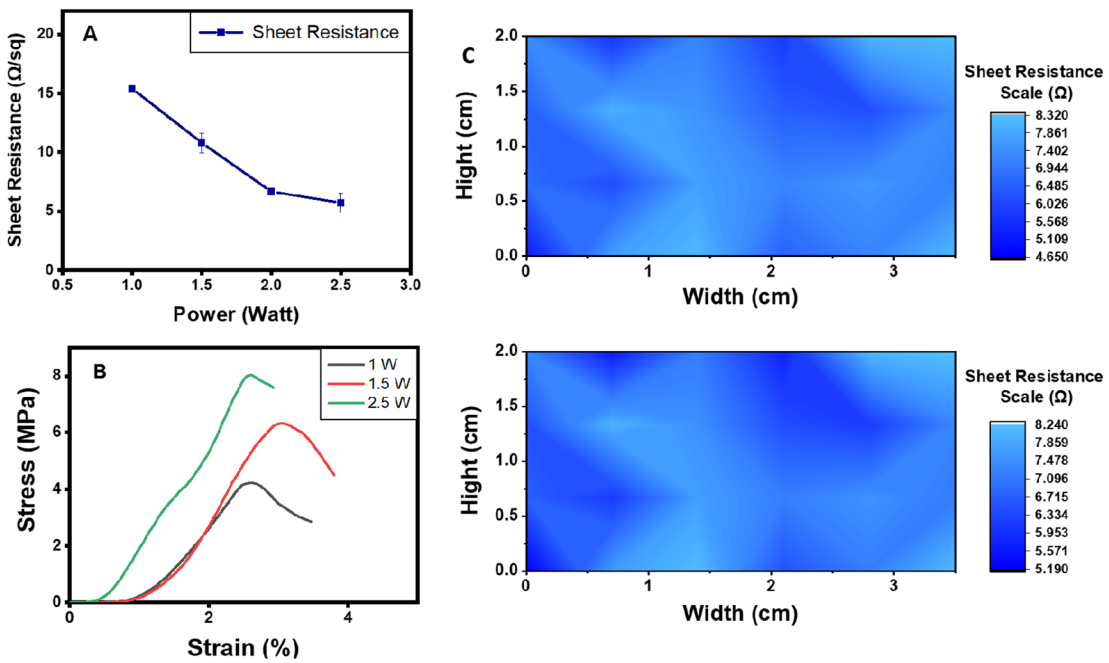

Fig. 7 Optimization of laser parameters. (A) Sheet resistance, (B) stress/strain curves of LIG-SF electrodes produced by different laser power, and (C) homogeneity of optimized LIG-SF electrodes determined by sheet resistance mapping of top and bottom layers.

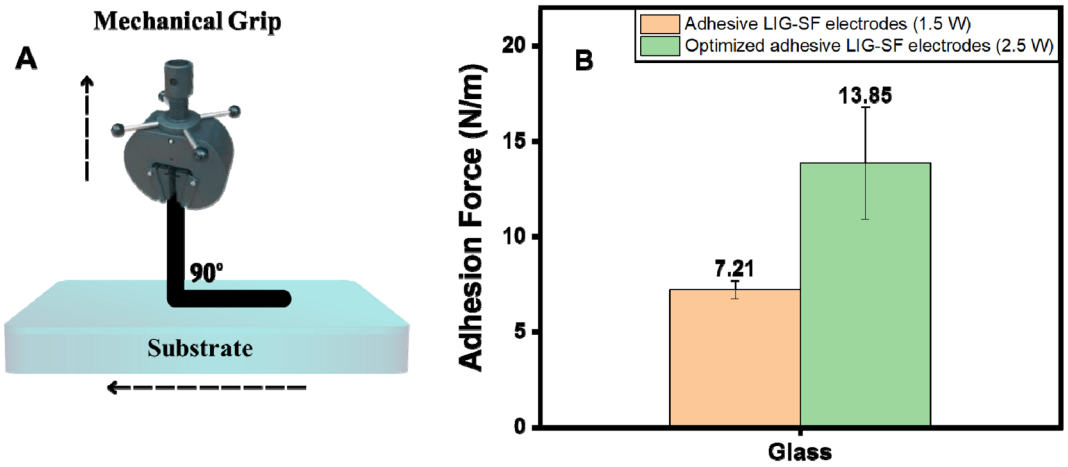

Fig. 8 (A) Adhesion force measurement setup, and (B) adhesion properties of adhesive LIG-SF electrodes.

structures were observed in C-SF treated at 900 °C in a CVD (Fig. 6A). The similar structure of micro-hole formation confirms the efficiency of our laser treatment procedure to produce LIG-SF electrodes at high temperatures. However, the mechanical properties and wight loss % yielded from both carbonization approaches were different. CVD C-SF showed a maximum tensile strength of 3.35 MPa and a maximum strain at break of 5.4%, while the maximum tensile strength and strain at break of muffle C-SF reached 12.6 MPa and 26.15%, respectively (Fig. 6C). Moreover, weight loss % of both carbonization approaches were evaluated after carbonization. CVD C-SF showed a weight loss of 85.39%, where muffle C-SF showed a weight loss of 69.34% only (Fig. 6). Based on the results provided in Fig. 6, muffle C-SF showed the same microstructure as CVD C-SF while maintaining better mechanical properties and a reasonable weight loss %, subsequently, can be a preferred candidate for wearable electrophysiological signals recording electrodes.

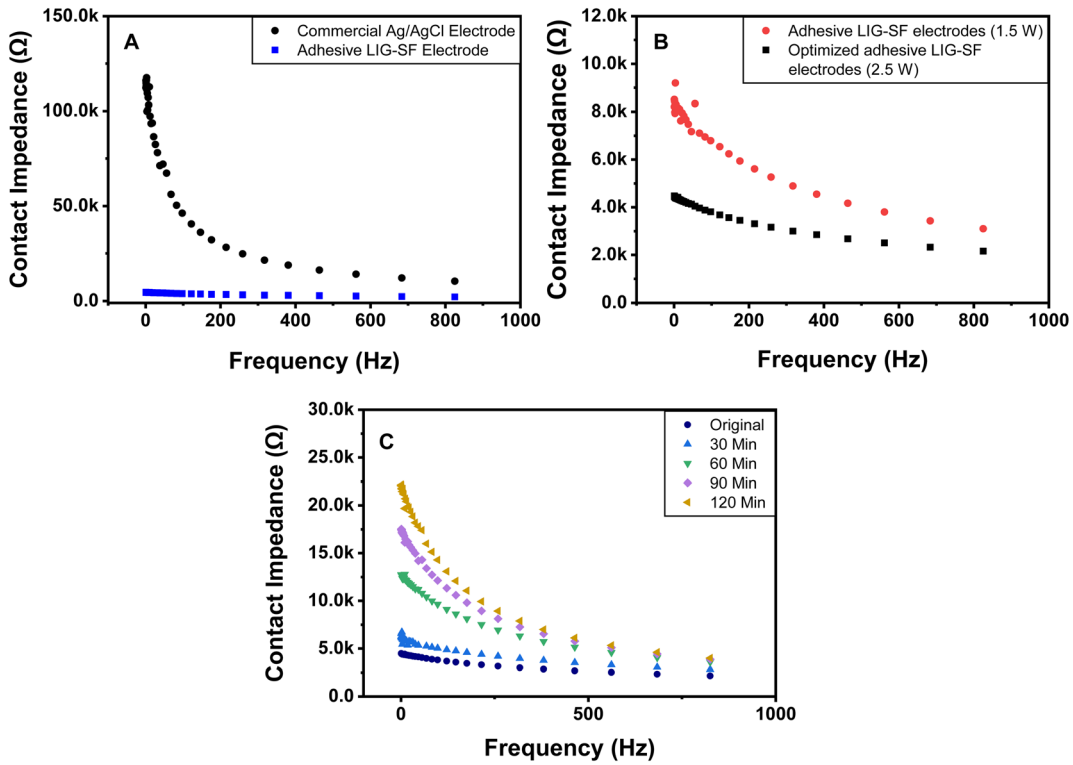

Fig. 9 Electrode-skin contact impedance. (A) Comparison of commercial Ag/AgCl electrodes with adhesive LIG-SF electrodes, (B) contact impedance of adhesive LIG-SF electrodes fabricated with different laser treatment power, and (C) contact impedance of adhesive LIG-SF electrodes during long-time attachment with human skin.

Table 2 Comparison of the characteristics of our developed adhesive LIG-SF electrodes with other similar previously developed electrodes

Wearable electrode	Description	Flexibility	Sheet resistance (Ω sq^{-1})	Contact impedance at (kΩ@10–40 Hz)	Ref.
Ag/AgCl	Commercial silver/silver chloride	Non-flexible	N/A	~80–120	Commer-cial
PEDOT: PSS/LIG	Spray coated conductive polymer on LIG	Flexible	17.4	~385	54
CRGO/Nylon membrane	Thermally reduced graphene oxide-nylon membrane	Flexible	40	~20	15
CAPE	Conformal and adhesive polymer electrodes	Flexible	N/A	2.8	44
Ppy@AM-SF/CNC	Polypyrrole and acid modified silk (AM-SF)/cellulose nanocrystals (CNC) films	Flexible	N/A	10–100	45
Adhesive LIG-SF	Adhesive LIG on silk fabrics	Flexible	5	4	This work

The weight loss of approximately 69.34% of C-SF can be related to the mass loss for silkworm silk occurred during the thermal treatment between 250 and 300 °C, reflecting the transition of silk proteins from unstable random coil structures to a stable β-sheet crystal structure, followed by the transformation of β-sheet structures into sp^2-hybridized carbon hexagonal structures 350 °C.[55,64] Moreover, as previously indicated by Raman spectroscopy, C-SF samples heated at 350 °C revealed a pseudographitic crystalline structure, with two distinctive carbon characteristic peaks at ~1350 and ~1580 cm^{-1}, corresponding to (D band) and (G band), respectively with the disappearance of silk protein B-sheet peaks of untreated P-SF samples (Fig. 5), indicating the effective carbonization of the silk fabrics.

3.3. Laser treatment of SFs

3.3.1. Optimization of laser processing parameters. Structural preservation, mechanical properties and sheet resistance of the fabricated LIG-SF electrodes are intensely correlated to laser processing parameters. Sheet resistance measurements of the fabricated LIG-SF electrodes were evaluated after treatment with different laser power varied from 1–2.5 watt. As shown in Fig. 7A, sheet resistance decreases with the increase of laser treatment power until reaching a minimum sheet resistance of 5.5 Ω/sq at a treatment power of 2.5 watt. This low sheet resistance can be attributed to the transformation of non-conductive C-SF into conductive laser induced graphene in LIG-SF electrodes *via* laser treatment. Mechanical strength of LIG-SF electrodes fabricated with different laser treatment power showed the same behavior.

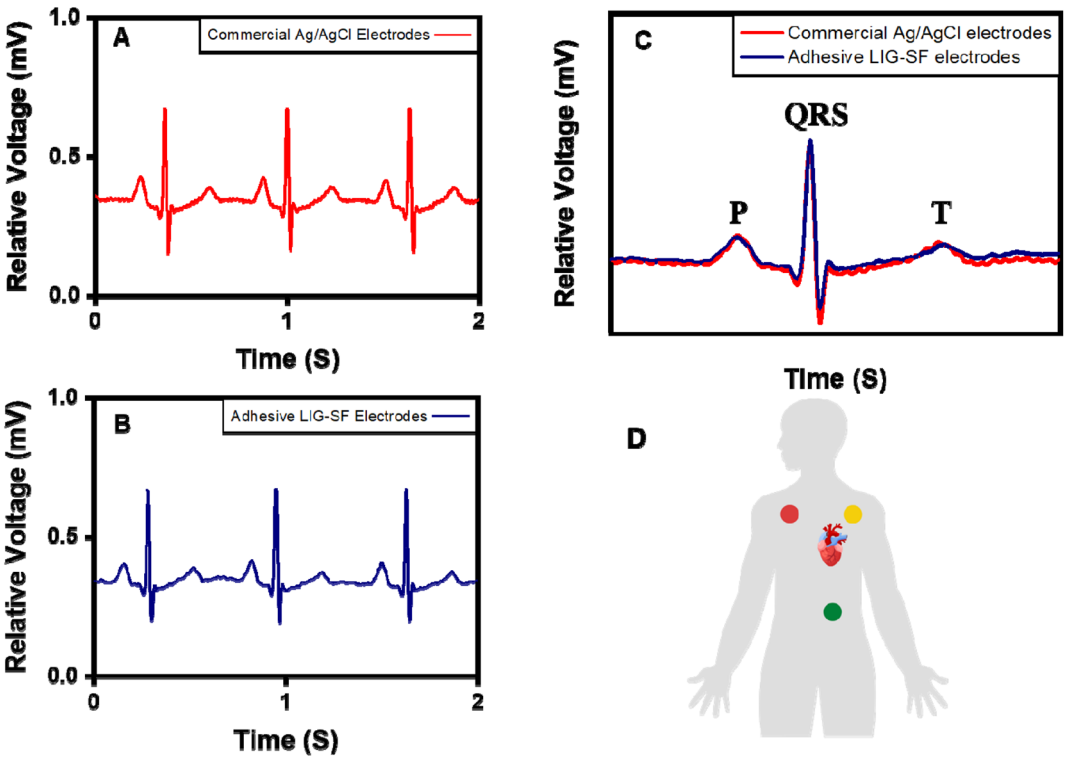

Fig. 10 Human biopotential recording. (A) ECG signals obtained by commercial Ag/AgCl electrodes, (B) ECG signals obtained by adhesive LIG-SF electrodes, (C) ECG waveform structure, and (D) placement of the three-electrode ECG recording system.

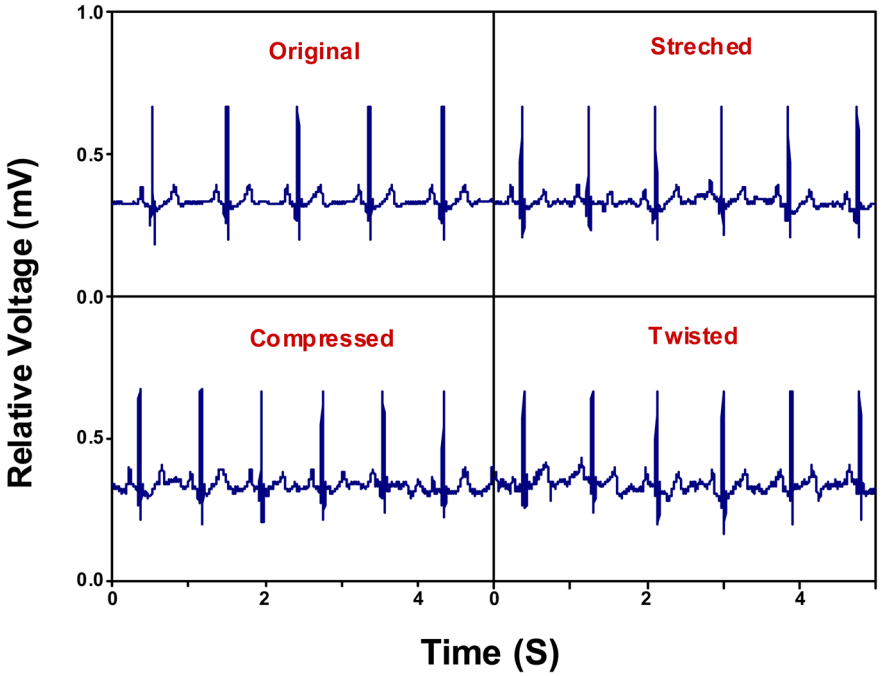

Fig. 11 ECG signals obtained by adhesive LIG-SF electrodes upon different skin deformations.

Where, the tensile strength of LIG-SF increased with the increase of laser treatment power to a maximum value of 8.03 MPa at a treatment power of 2.5 watt (Fig. 7B). Therefore, LIG-SF electrodes produced at a treatment power of 2.5 watt showed a minimum sheet resistance (5.5 Ω sq^{-1}) while maintaining the mechanical properties of SFs. The mechanical robustness of LIG-SF electrodes may be attributed to the interconnected fiber network structure of woven silk fabrics.

3.3.2. Homogeneity of LIG-SF electrodes. Fabrication of large-area LIG while maintaining the mechanical properties of SFs and with low sheet resistance of a high degree of homogeneity on both sides is highly challenging. Large-area LIG-SF electrodes of 35 mm in length and 20 mm in width were designed and fabricated with optimal parameters (a scanning speed of 30 mm s^{-1}, a laser path spacing of 0.2 mm, a focus distance of 10 mm, and laser treatment power of 2.5 watt). The homogeneity of top and bottom layers of LIG-SF electrodes were investigated by SEM, EDX and sheet resistance mapping. SEM images of the bottom layer of LIG-SF electrodes (Fig. S2A and C†) show the same micro-hole structures present in the top

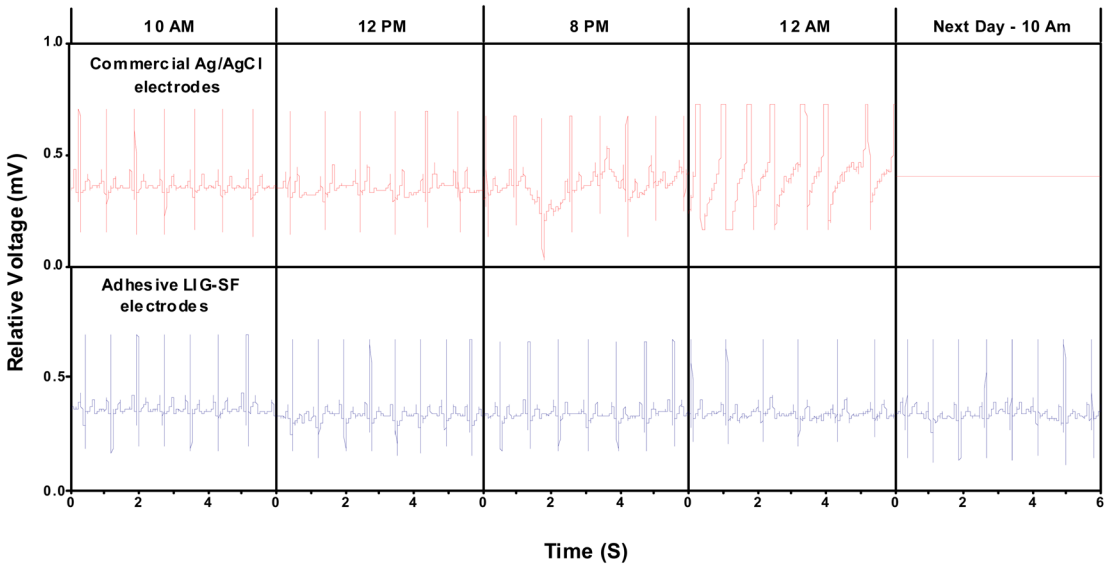

Fig. 12 ECG signals obtained over 24 h of attachment on volunteer's skin.

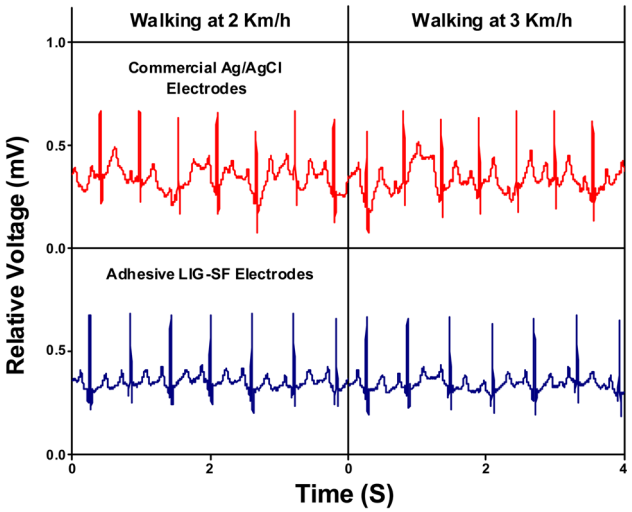

Fig. 13 ECG signals recording during walking at 2–3 km h^{-1} by commercial Ag/AgCl electrodes and adhesive LIG-SF electrodes.

layer of LIG-SF electrodes (Fig. 3C, F and I). Moreover, elemental atomic percentage ratios of both top and bottom layers of LIG-SF were calculated by EDX (Table 1). The atomic percentage ratios of carbon, nitrogen and oxygen were nearly equal in both top and bottom layers. In addition, sheet resistance was measured at different 24 points of each side covering the whole fabric surface in order to study the sheet resistance homogeneity of both top and bottom layers of LIG-SF electrodes. Fig. 7C shows the sheet resistance mapping of top and bottom layers of optimized LIG-SF electrodes. Apparently, evaluated sheet resistance values on both sides (Tables S1 and S2†) were in a narrow range of 4.5–8.3 Ω sq^{-1}, therefore, reflecting the sheet resistance homogeneity of optimized LIG-SF. These results of sheet resistance mapping and EDX atomic percentage ratio indicate the high degree of homogeneity of optimized LIG-SF electrodes.

3.4. Adhesion of LIG-SF electrodes

Adhesive properties of wearable epidermal electrodes play a vital role for providing high degree of conformity with human skin.[65,66] Unlike conventional Ag/AgCl electrodes, conformal adhesive electrodes provide a highly conformal and uniform contact with human skin at both, original and even at deformed skin states (Fig. S3†). Calcium-modified silk fibroin has been investigated as a biocompatible adhesive for epidermal electrodes due to metal–chelate complexes and water-capturing points induced by calcium ions-silk fibroin interaction.[65,67,68] Silk/Ca^{2+} adhesive solutions were prepared by dissolving in formic acid with a weight ratio of 70 : 30, cast on top of LIG-SF and then dried overnight to form adhesive LIG-SF electrodes. Adhesion forces of adhesive LIG-SF electrodes were evaluated *via* a standard 90°-peel test method (Fig. 8A). As shown in Fig. 8B, optimized adhesive LIG-SF electrodes showed a strong adhesion on glass substrates for up to 13.85 N m^{-1}. Adhesive properties of SF-LIG electrodes allowed a conformal contact to the body's shape, ensuring a comfortable fit for users during extended monitoring periods. This comfort encourages patient compliance and allow extended monitoring in long-term applications.

In addition, adhesion properties were investigated on adhesive LIG-SF electrodes fabricated by two different laser treatment powers (1.5 and 2.5 watt). As shown in (Fig. 8B), optimized adhesive LIG-SF electrodes fabricated at 2.5 watt showed higher adhesive forces (13.85 N m^{-1}) than adhesive LIG-SF electrodes fabricated at 1.5 watt (7.21 N m^{-1}). The high adhesive forces of optimized LIG-SF electrodes may be attributed to the micro-hole structure induced by

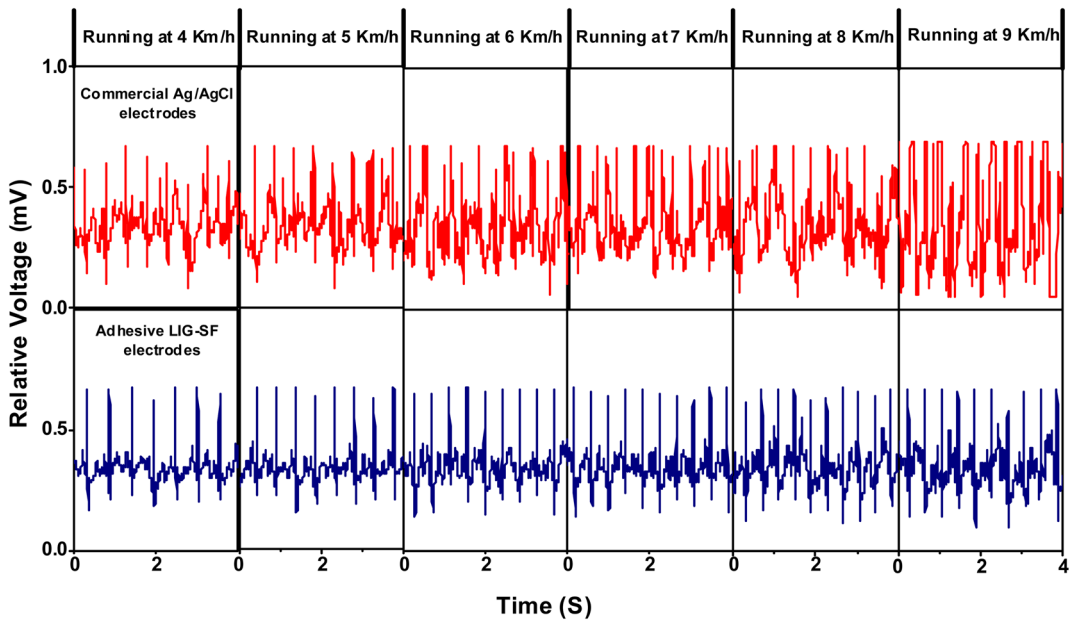

Fig. 14 ECG signals recording during running at different running speeds by commercial Ag/AgCl electrodes and adhesive LIG-SF electrodes.

laser treatment at 2.5 watt (Fig. 3I). In case of LIG-SF electrodes (1.5 watt), laser treatment power was insufficient for the formation of micro-hole structures, instead, GO aggregates were formed on surface of SFs (Fig. S2B and D†). The micro-hole surface structures provided a mechanical interlocking adhesion that led to higher adhesion forces in case of optimized LIG-SF electrodes.[69] Therefore, the adhesion of optimized adhesive LIG-SF electrodes is controlled by two main mechanisms, adsorption of silk/Ca^{+2} layer onto the surface of LIG-SF electrodes and also by the mechanical interlocking adhesion induced by the micro-hole porous structures in contact with LIG-SF electrodes (Fig. S4†).

3.5. Electrode-skin contact impedance

Electrode-skin contact impedance is the impedance formed at an electrode-skin interface.[70] To obtain a stable and high-quality electrophysiological signal recording, low electrode-skin contact impedance as well as high conductivity are required.[71] Signal amplitude, contact duration and frequency range are the three main parameters that can affect the impedance at the electrode-skin interface. Electrode-skin contact impedance was measured on a volunteer's forearm in the frequency range of 1–1000 Hz and at a signal amplitude of 0.05 V. Compared with commercial Ag/AgCl electrodes, adhesive LIG-SF electrodes had much lower contact impedance specially in the frequency range of 1–40 Hz (Fig. 9A), which mainly responsible for ECG collection.[72,73] The low electrode-skin contact impedance of adhesive LIG-SF electrodes may be attributed to the highly self-adhesive capability and the very low sheet resistance (5.5 Ω sq^{-1}) achieved by laser treatment.

Electrode-skin contact impedance were studied for LIG-SF electrodes fabricated by two different laser treatment powers (1.5 and 2.5 watt). As previously discussed for adhesion properties, the micro-hole surface structures led to higher adhesion forces in case of optimized LIG-SF electrodes. Therefore, it was expected that optimized adhesive LIG-SF electrodes would consequently have a lower electrode-skin contact impedance (Fig. 9B). In addition, electrode-skin contact impedance of adhesive LIG-SF electrodes were investigated over a long period of attachment with human skin (Fig. 9C). Electrode-skin contact impedance slightly increased with the increase in time, hence, confirming the reliability and applicability of adhesive LIG-SF electrodes for long-term performance.

Eventually, Table 2 summarizes and compares the characteristics of adhesive LIG-SF electrodes with other similar previously developed electrodes. As a conclusion, our developed adhesive LIG-SF electrodes has excellent characteristics in comparison with other electrodes reported so far. Therefore, our proposed adhesive LIG-SF electrodes are excellent candidates for electrophysiological monitoring applications.

3.6. Electrophysiological signals recording

ECG signals arise from the electrical changes induced by depolarization and repolarization of heart muscles therefore, they are vital in pathological disease diagnosis of CVDs.[74] In order to study the ability of adhesive LIG-SF electrodes for electrophysiological signals recording, ECG signals of a volunteer (Male, 25 years old) were recorded by a three-electrode system (Fig. 10D) at different body status such as resting, running and over one day of activity. ECG signals were successfully obtained by adhesive LIG-SF electrodes at resting states and were comparable with those obtained by commercial Ag/AgCl electrodes (Fig. 10A and B). Both types of electrodes were attached to a volunteer's chest to measure ECG electrophysiological signals with a complete normal ECG waveform structure composed of P waves, QRS complex, and T waves as shown in Fig. 10C.[75] In order to investigate the capability of adhesive LIG-SF electrodes to detect ECG signals upon skin deformations, ECG signals were obtained by adhesive LIG-SF electrodes with high stability while stretching, squeezing and twisting the skin (Fig. 11).

Moreover, adhesive LIG-SF electrodes were investigated for long-term ECG monitoring through obtaining ECG signals continuously for 24 h of attachment on volunteer's skin. ECG signals were recorded at different periods in the same day to ensure obtaining ECG signals at normal daily-life activities of the volunteer (Fig. 12). In case of commercial Ag/AgCl electrodes, ECGs obtained were stable for the first 6 hours of attachment. However, after 10 hours of attachment, ECG signals were slightly unstable. ECG signals obtained after 14 hours became completely deteriorated and electrodes started to fall from the skin. The next day, after 24 hours of attachment, electrodes fell completely from the skin and no ECG signals were obtained. On the other hand, ECG signals obtained by adhesive LIG-SF electrodes were highly stable for 24 hours. Therefore, the developed adhesive SF-LIG electrodes are suitable for long-term monitoring, subsequently, they can be applied for stable and continuous long-term healthcare monitoring, providing a comprehensive view of an individual's electrophysiological activities.

Furthermore, the capability of both commercial Ag/AgCl and adhesive LIG-SF electrodes was investigated for ECG recording during body movement. In order to control the movement

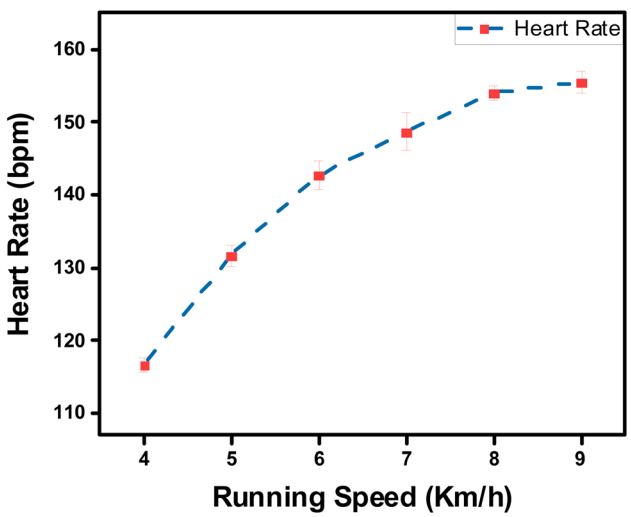

Fig. 15 Exercise heart rate at different running speeds obtained by adhesive LIG-SF electrodes.

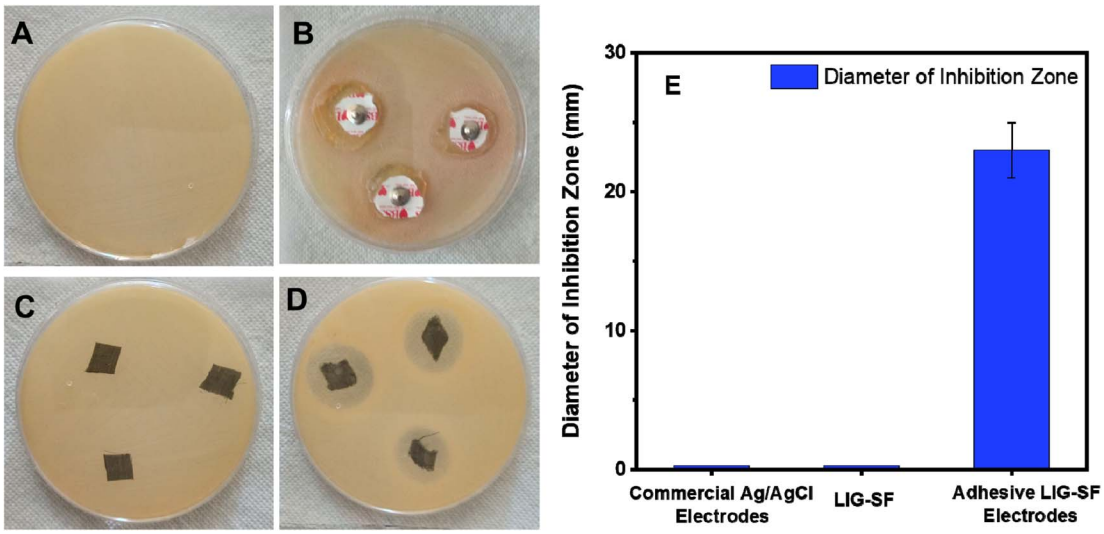

Fig. 16 Anti-bacterial properties. (A–D) digital photographs of *S. aureus*-cultured colonies of control, commercial Ag/AgCl, LIG-SF and adhesive LIG-SF electrodes, respectively. (E) Diameter of bacterial inhibition zone after 24 h of incubation.

intensity, a treadmill (Model 550 Ti, Intenza Fitness) was utilized for body movement experiments where both types of electrodes were attached onto the volunteer's chest. ECG signals were recorded during walking at 2–3 km h^{-1} showed that ECG signals obtained by adhesive LIG-SF electrodes were more stable than those obtained by commercial Ag/AgCl electrodes (Fig. 13). With increasing movement intensity, ECG signals were recorded at different running speeds ranging from 4 to 9 km h^{-1} (Fig. 14). In case of commercial Ag/AgCl electrodes, ECG signals were unstable in at low running speeds (4–6 km h^{-1}). However, ECG signals were completely deteriorated with no obvious ECG waveform structure with the increase in running speed from 7–9 km h^{-1}. The unstable ECG recording of commercial Ag/AgCl electrodes during motion artifacts may be attributed to the volatilization of the liquid conductive gel and the increase of contact impedance between the electrode and human skin.[12,76] Contrastingly, ECG signals obtained by adhesive LIG-SF electrodes were highly stable at low running speeds (4–6 km h^{-1}). Moreover, at high running speeds (7–9 km h^{-1}), ECG signals obtained by adhesive LIG-SF electrodes were much more stable than those recorded by commercial Ag/AgCl electrodes. The high stability of ECG recording obtained by adhesive LIG-SF electrodes can be attributed to the flexibility, conformal contact and the high adhesion to human skin that overcome motion artifacts even during intense body movements. In addition, ECG recording at different walking and running speeds can be an indicator for calculating a target heart rate to maximize athlete's workouts through an exercise heart rate chart. Therefore, heart rate at different running speeds was calculated from ECG recordings as shown in Fig. 15. Exercise heart rate increased with the increase in running speed until reach 145–160 beats per minute (bpm) at high running speeds (7–9 km h^{-1}) matching 60–70% of maximum heart rate which are optimal for weight loss applications.[77,78] Therefore, adhesive LIG-SF electrodes enable ambulatory monitoring, allowing patients to move freely while recording essential electrophysiological data. Therefore, adhesive SF-LIG electrodes can be applicable for several health conditions that require continuous monitoring, such as cardiac arrhythmias, and for sports management applications.

3.7. Anti-bacterial properties of adhesive LIG electrodes

Electrophysiological flexible wearable electrodes are directly attached onto human skin therefore, anti-bacterial properties are preferred to prevent bacterial infection that may be induced by the organic matter in sweat.[79] Anti-bacterial activity of commercial Ag/AgCl, LIG-SF and adhesive LIG-SF electrodes were studied using Gram-positive *S. aureus via* Kirby–Bauer test[57]. After incubation for 24 h, it was observed that commercial Ag/AgCl has no antibacterial activity (Fig. 16B). In case of LIG-SF electrodes, after laser treatment, no antibacterial activity was observed (Fig. 16C). However, after coating with silk fibroin/calcium ions adhesive layer, adhesive LIG-SF electrodes showed an excellent anti-bacterial activity against *S. aureus* (Fig. 16D) with an inhibition zone diameter of 23 mm (Fig. 16E). The excellent anti-bacterial activity of adhesive LIG-SF electrodes can be attributed to the anti-bacterial properties of silk fibroin/calcium ions adhesive layer. The antibacterial properties of LIG-SF electrodes is crucial to minimize the potential for skin irritation, redness, or rashes that can occur when microorganisms proliferate on the electrode's surface.

4. Conclusions

Herein, an anti-bacterial and self-adhesive silk-based LIG electrodes for electrophysiological monitoring *via* a facile and cost-effective approach. LIG on SFs were achieved by a two-step carbonization method. First, natural SFs were carbonized in a conventional muffle furnace at 350 °C for 3 h and then the produced non-conductive carbonized SFs were laser treated by a CO_2-pulsed laser to form a highly conductive LIG-SF. Finally, adhesive LIG-SF electrodes with adhesive forces of 13.85 N m^{-1}

on glass substrates were prepared by casting of silk/Ca^{2+}/F.A solution onto LIG-SF. Double-sided homogeneity of LIG-SF with a minimum sheet resistance of 5.5 Ω sq^{-1} were achieved *via* optimization of laser processing parameters. Moreover, adhesive LIG-SF electrodes showed a much lower electrode-skin contact impedance compared to conventional Ag/AgCl electrodes, thus, providing high stability of electrophysiological signals recording. Adhesive LIG-SF electrodes showed an excellent performance with high stable ECG signals recording while walking, running at different speeds from 4–9 km h^{-1} and also at long-term ECG monitoring over a day. Therefore, adhesive LIG-electrodes are potential candidates for smart healthcare and smart sports management applications.

Conflicts of interest

There are no conflicts to declare.

Acknowledgements

Authors would like to thank the Physical fitness, Locomotor rehabilitation and Physiological measurement Unit at Fayoum University for facilitating the performance of the physical activities required for stress ECG experiments.

References

1 J. Rettinger, *et al.*, *Electrophysiology: Basics, Methods, Modern Approaches and Applications*, Springer Nature, 2022.
2 J. S. Barlow, *The electroencephalogram: its patterns and origins*, MIT press, 1993.
3 R. J. Martis, U. R. Acharya and H. Adeli, Current methods in electrocardiogram characterization, *Comput. Biol. Med.*, 2014, **48**, 133–149.
4 Y. J. Hong, *et al.*, Wearable and implantable devices for cardiovascular healthcare: from monitoring to therapy based on flexible and stretchable electronics, *Adv. Funct. Mater.*, 2019, **29**(19), 1808247.
5 K. Kompoliti, and V. Leonard, *Encyclopedia of movement disorders*, vol. 1, Academic Press, 2010.
6 M. Zhu, *et al.*, Flexible electrodes for in vivo and in vitro electrophysiological signal recording, *Adv. Healthcare Mater.*, 2021, **10**(17), 2100646.
7 Y. Fu, *et al.*, Dry electrodes for human bioelectrical signal monitoring, *Sensors*, 2020, **20**(13), 3651.
8 S. Imani, *et al.*, A wearable chemical–electrophysiological hybrid biosensing system for real-time health and fitness monitoring, *Nat. Commun.*, 2016, **7**(1), 1–7.
9 T. Yamaguchi, *et al.*, Cardiac dopamine D1 receptor triggers ventricular arrhythmia in chronic heart failure, *Nat. Commun.*, 2020, **11**(1), 1–8.
10 D. J. Lemos, and T. Omland, *Chronic coronary artery disease: A companion to Braunwald's heart disease E-Book*, 2017.
11 World Health Organization, *Cardiovascular Diseases (CVDs). Who.int; World Health Organization*, WHO, 2021, June 11, **https://www.who.int/news-room/fact-sheets/detail/cardiovascular-diseases-(cvds)**.
12 A. J. Portelli and S. J. Nasuto, Design and development of non-contact bio-potential electrodes for pervasive health monitoring applications, *Biosensors*, 2017, **7**(1), 2.
13 X. Du, *et al.*, Highly adhesive, washable and stretchable on-skin electrodes based on polydopamine and silk fibroin for ambulatory electrocardiography sensing, *J. Mater. Chem. C*, 2020, **8**(35), 12257–12264.
14 Y. Ma, *et al.*, Flexible hybrid electronics for digital healthcare, *Adv. Mater.*, 2020, **32**(15), 1902062.
15 P. S. Das, S. H. Park, K. Y. Baik, J. W. Lee and J. Y. Park, Thermally reduced graphene oxide-nylon membrane based epidermal sensor using vacuum filtration for wearable electrophysiological signals and human motion monitoring, *Carbon*, 2020, **158**, 386–393.
16 S. Chen, *et al.*, Flexible wearable sensors for cardiovascular health monitoring, *Adv. Healthcare Mater.*, 2021, **10**(17), 2100116.
17 M. Ha, S. Lim and H. Ko, Wearable and flexible sensors for user-interactive health-monitoring devices, *J. Mater. Chem. B*, 2018, **6**(24), 4043–4064.
18 S. Choi, *et al.*, Recent advances in flexible and stretchable bio-electronic devices integrated with nanomaterials, *Adv. Mater.*, 2016, **28**(22), 4203–4218.
19 W. Wu and H. Haick, Materials and wearable devices for autonomous monitoring of physiological markers, *Adv. Mater.*, 2018, **30**(41), 1705024.
20 S. Hozumi, S. Honda, T. Arie, S. Akita and K. Takei, Multimodal wearable sensor sheet for health-related chemical and physical monitoring, *ACS Sens.*, 2021, **6**(5), 1918–1924.
21 H. Wu, *et al.*, Materials, devices, and systems of on-skin electrodes for electrophysiological monitoring and human–machine interfaces, *Adv. Sci.*, 2021, **8**(2), 2001938.
22 C. Ji, *et al.*, Ultrathin-metal-film-based transparent electrodes with relative transmittance surpassing 100, *Nat. Commun.*, 2020, **11**(1), 1–8.
23 B. Xu, *et al.*, An epidermal stimulation and sensing platform for sensorimotor prosthetic control, management of lower back exertion, and electrical muscle activation, *Adv. Mater.*, 2016, **28**(22), 4462–4471.
24 N. Karim, S. Afroj, A. Malandraki, S. Butterworth, C. Beach, M. Rigout, S. G. Yeates, *et al.*). All inkjet-printed graphene-based conductive patterns for wearable e-textile applications, *J. Mater. Chem. C*, 2017, **5**(44), 11640–11648.
25 A. Kolanowska, A. P. Herman, R. G. Jędrysiak and S. Boncel, Carbon nanotube materials for electrocardiography, *RSC Adv.*, 2021, **11**(5), 3020–3042.
26 Z. Li, *et al.*, On-skin graphene electrodes for large area electrophysiological monitoring and human-machine interfaces, *Carbon*, 2020, **164**, 164–170.
27 L. Eskandarian, A. Toossi, F. Nassif, S. Golmohammadi Rostami, S. Ni, A. Mahnam, H. E. Naguib, *et al.*). 3D-Knit Dry Electrodes using Conductive Elastomeric Fibers for Long-Term Continuous Electrophysiological Monitoring, *Adv. Mater. Technol.*, 2022, **7**(7), 2101572.
28 W. Guo, *et al.*, Matrix-independent highly conductive composites for electrodes and interconnects in stretchable

electronics, *ACS Appl. Mater. Interfaces*, 2019, **11**(8), 8567–8575.

29 J. Ferri, R. Llinares, I. Segarra, A. Cebriánv, E. Garcia-Breijo and J. Millet, A new method for manufacturing dry electrodes on textiles. Validation for wearable ECG monitoring, *Electrochem. Commun.*, 2022, **136**, 107244.

30 L. Zhang, *et al.*, Fully organic compliant dry electrodes self-adhesive to skin for long-term motion-robust epidermal biopotential monitoring, *Nat. Commun.*, 2020, **11**(1), 1–13.

31 L. Xu, S. Liu, L. Zhu, Y. Liu, N. Li, X. Shi, Z. Qin, *et al.*). Hydroxypropyl methyl cellulose reinforced conducting polymer hydrogels with ultra-stretchability and low hysteresis as highly sensitive strain sensors for wearable health monitoring, *Int. J. Biol. Macromol.*, 2023, 123956.

32 J. C. Hsieh, Y. Li, H. Wang, M. Perz, Q. Tang, K. W. K. Tang, H. Wang, *et al.*). Design of hydrogel-based wearable EEG electrodes for medical applications, *J. Mater. Chem. B*, 2022, **10**(37), 7260–7280.

33 L. You, X. Shi, J. Cheng, J. Yang, C. Xiong, Z. Ding, J. Wang, *et al.*). Flexible porous Gelatin/Polypyrrole/Reduction graphene oxide organohydrogel for wearable electronics, *J. Colloid Interface Sci.*, 2022, **625**, 197–209.

34 Y. Zhao, *et al.*, Ultra-conformal skin electrodes with synergistically enhanced conductivity for long-time and low-motion artifact epidermal electrophysiology, *Nat. Commun.*, 2021, **12**(1), 1–12.

35 S. Yoon, *et al.*, Multifunctional hybrid skin patch for wearable smart healthcare applications, *Biosens. Bioelectron.*, 2022, **196**, 113685.

36 P. A. Lopes, *et al.*, Soft bioelectronic stickers: selection and evaluation of skin-interfacing electrodes, *Adv. Healthcare Mater.*, 2019, **8**(15), 1900234.

37 H. Tabasum, N. Gill, R. Mishra and S. Lone, Wearable microfluidic-based e-skin sweat sensors, *RSC Adv.*, 2022, **12**(14), 8691–8707.

38 Qi Wang, *et al.*, Self-healable multifunctional electronic tattoos based on silk and graphene, *Adv. Funct. Mater.*, 2019, **29**(16), 1808695.

39 J. Han, *et al.*, Electrospun core–shell nanofibrous membranes with nanocellulose-stabilized carbon nanotubes for use as high-performance flexible supercapacitor electrodes with enhanced water resistance, thermal stability, and mechanical toughness, *ACS Appl. Mater. Interfaces*, 2019, **11**(47), 44624–44635.

40 Z. Xu, *et al.*, A Highly-Adhesive and Self-Healing Elastomer for Bio-Interfacial Electrode, *Adv. Funct. Mater.*, 2021, **31**(1), 2006432.

41 X. Liu, *et al.*, Bioinspired, microstructured silk fibroin adhesives for flexible skin sensors, *ACS Appl. Mater. Interfaces*, 2020, **12**(5), 5601–5609.

42 Y. Cao and B. Wang, Biodegradation of silk biomaterials, *Int. J. Mol. Med. Adv. Sci.*, 2009, **10**(4), 1514–1524.

43 X. Liang, *et al.*, Stable and biocompatible carbon nanotube ink mediated by silk protein for printed electronics, *Adv. Mater.*, 2020, **32**(31), 2000165.

44 H. Yang, *et al.*, Adhesive biocomposite electrodes on sweaty skin for long-term continuous electrophysiological monitoring, *ACS Mater. Lett.*, 2020, **2**(5), 478–484.

45 L. Meng, *et al.*, Self-adhesive, biodegradable silk-based dry electrodes for epidermal electrophysiological monitoring, *Chem. Eng. J.*, 2022, **427**, 131999.

46 Z. Lu, *et al.*, In situ synthesis of silver nanoparticles uniformly distributed on polydopamine-coated silk fibers for antibacterial application, *J. Colloid Interface Sci.*, 2015, **452**, 8–14.

47 C. Wang, *et al.*, Carbonized SF for ultrastretchable, highly sensitive, and wearable strain sensors, *Adv. Mater.*, 2016, **28**(31), 6640–6648.

48 Z. Lu, *et al.*, SF-based wearable thermoelectric generator for energy harvesting from the human body, *Appl. Energy*, 2016, **164**, 57–63.

49 J. Zhou, *et al.*, Multi-walled carbon nanotubes functionalized SFs for mechanical sensors and heating materials, *Mater. Des.*, 2020, **191**, 108636.

50 W. Lu, *et al.*, Molybdenum disulfide nanosheets aligned vertically on carbonized SF as smart textile for wearable pressure-sensing and energy devices, *ACS Appl. Mater. Interfaces*, 2020, **12**(10), 11825–11832.

51 X. Song, *et al.*, A graphene-coated silk-spandex fabric strain sensor for human movement monitoring and recognition, *Nanotechnology*, 2021, **32**(21), 215501.

52 F. M. Vivaldi, A. Dallinger, A. Bonini, N. Poma, L. Sembranti, D. Biagini, P. Salvo, F. Greco and F. Di Francesco, Three-dimensional (3D) laser-induced graphene: structure, properties, and application to chemical sensing, *ACS Appl. Mater. Interfaces*, 2021, **13**(26), 30245–30260.

53 Z. Li, *et al.*, Preparation of Laser-Induced Graphene Fabric from Silk and Its Application Examples for Flexible Sensor, *Adv. Eng. Mater.*, 2021, **23**(9), 2100195.

54 M. A. Zahed, *et al.*, Flexible and robust dry electrodes based on electroconductive polymer spray-coated 3D porous graphene for long-term electrocardiogram signal monitoring system, *Carbon*, 2020, **165**, 26–36.

55 Se Y. Cho, *et al.*, Carbonization of a stable β-sheet-rich silk protein into a pseudographitic pyroprotein, *Nat. Commun.*, 2015, **6**(1), 1–7.

56 A. Elbaki, K. M. Mohamed, R. M. G. Ahmed and S. G. K. Ahmed, Silk-based 2D nanocomposites for superior oily wastewater remediation, *J. Cleaner Prod.*, 2022, **365**, 132707.

57 H. S. Bhargav, *et al.*, Measurement of the zone of inhibition of an antibiotic, *2016 IEEE 6th International Conference on Advanced Computing (IACC)*, IEEE, 2016.

58 Y. Liang, D. Wu and R. Fu, Carbon microfibers with hierarchical porous structure from electrospun fiber-like natural biopolymer, *Sci. Rep.*, 2013, **3**(1), 1–5.

59 P. Monti, *et al.*, Raman spectroscopic studies of silk fibroin from Bombyx mori, *J. Raman Spectrosc.*, 1998, **29**(4), 297–304.

60 D. Puchowicz, & M. Cieslak, Raman spectroscopy in the analysis of textile structures, *Recent developments in atomic force microscopy and Raman spectroscopy for materials characterization*, 2022, pp. 1–21.

61 F. Mahmood, C. Zhang, Y. Xie, D. Stalla, J. Lin and C. Wan, Transforming lignin into porous graphene via direct laser writing for solid-state supercapacitors, *RSC Adv.*, 2019, **9**(39), 22713–22720.
62 B. Anis, A. Abouelsayed, A. M. Sawy and A. S. Khalil, Tuning the plasmon resonance and work function of laser-scribed chemically doped graphene, *Carbon*, 2017, **120**, 44–53.
63 *Activated carbon fiber and textiles*, J. Y. Chen, Woodhead Publishing, 2016.
64 X. Chen, Z. Shao, D. P. Knight and F. Vollrath, Conformation transition kinetics of Bombyx mori silk protein, *Proteins: Struct., Funct., Bioinf.*, 2007, **68**(1), 223–231.
65 J. -W. Seo, *et al.*, Calcium-modified silk as a biocompatible and strong adhesive for epidermal electronics, *Adv. Funct. Mater.*, 2018, **28**(36), 1800802.
66 Y. J. Hong, *et al.*, Wearable and implantable devices for cardiovascular healthcare: from monitoring to therapy based on flexible and stretchable electronics, *Adv. Funct. Mater.*, 2019, **29**(19), 1808247.
67 S. Ling, *et al.*, Printing of stretchable silk membranes for strain measurements, *Lab Chip*, 2016, **16**(13), 2459–2466.
68 N. Drnovšek, *et al.*, Size of silk fibroin β-sheet domains affected by Ca 2+, *J. Mater. Chem. B*, 2016, **4**(40), 6597–6608.
69 W.-S. Kim, *et al.*, Evaluation of mechanical interlock effect on adhesion strength of polymer–metal interfaces using micro-patterned surface topography, *Int. J. Adhes. Adhes.*, 2010, **30**(6), 408–417.
70 G. Li, S. Wang and Y. Y. Duan, Towards gel-free electrodes: A systematic study of electrode-skin impedance, *Sens. Actuators, B*, 2017, **241**, 1244–1255.
71 L. Yang, *et al.*, Insight into the Contact Impedance between the Electrode and the Skin Surface for Electrophysical Recordings, *ACS Omega*, 2022, **7**(16), 13906–13912.
72 O. Terán-Jiménez, *et al.*, Sensors based on conducting polymers for measurement of physiological parameters, *IEEE Sens. J.*, 2017, **17**(8), 2492–2497.
73 B. Chandrakar, O. P. Yadav and V. K. Chandra, A survey of noise removal techniques for ECG signals, *Int. J. Adv. Comput. Res. Commun. Eng.*, 2013, **2**(3), 1354–1357.
74 M. Elgendi, A. Mohamed and R. Ward, Efficient ECG compression and QRS detection for e-health applications, *Sci. Rep.*, 2017, **7**(1), 1–16.
75 G. S. Wagner, *et al.*, Interpretation of the normal electrocardiogram, *Marriott's practical electrocardiography*, vol. 9, 2008, p. 50.
76 H.-L. Peng, *et al.*, Parylene-based flexible dry electrode for bioptential recording, *Sens. Actuators, B*, 2016, **231**, 1–11.
77 J. Achten and E. Asker, Jeukendrup. "Heart rate monitoring, *Sports Med.*, 2003, **33**(7), 517–538.
78 R. L. Gellish, *et al.*, Longitudinal modeling of the relationship between age and maximal heart rate, *Med. Sci. Sports Exercise*, 2007, **39**(5), 822–829.
79 L. Teufel, *et al.*, Material-dependent growth of human skin bacteria on textiles investigated using challenge tests and DNA genotyping, *J. Appl. Microbiol.*, 2010, **108**(2), 450–461.